Journal of Nanobiotechnology

RESEARCH Open Access

Integration of bioinformatics analysis and experimental verification reveals the role of neutrophil extracellular traps in silica nanoparticles-induced lung injury

Xiu He[1*†], Xiaoli Yuan[1†], Xuedong Sa[1†], Jiaqi Ban[1], Shuai Fu[1], Mingdan You[1] and Jun Li[1*]

Abstract

Background Silica nanoparticles (SiNPs) are extensively produced and utilized, leading to regular human exposure in both living environmental and occupational settings. Numerous studies have confirmed the detrimental effects of SiNPs on respiratory health. Neutrophil extracellular traps (NETs), web-like networks of DNA, histones, and antimicrobial proteins that neutrophils release to trap and kill pathogens, are implicated in development of some acute and chronic lung diseases. Nevertheless, the specific role of NETs in the adverse pulmonary effects of SiNPs has not been described.

Methods Male C57BL/6 mice received intratracheal instillation of 80 nm SiNPs at 3.0 and 6.0 mg/kg body weight (bw), once weekly for 12 weeks, to simulate actual occupational exposure scenarios. Combined with bioinformatics analysis, this exploratory study investigated SiNPs-induced lung injury and the impact on metrics related to NETs. Subsequently, DNase I was used to explore the mitigating effect and mechanisms of promoting NETs degradation on SiNPs-induced lung injury. The DNase I was administered at a dose of 300 U per mouse via intraperitoneal injection, three times a week for 12 weeks.

Results Exposure to SiNPs induced pulmonary injury in C57BL/6 mice. Results of bioinformatic analyses and molecular bioassay techniques revealed that NETs, integrins αLβ2 and αMβ2, CD44, TGF-β and cytokines participate in SiNPs-induced lung injury. Targeted inhibition of NETs via DNase I attenuated the overexpression of integrins, CD44 and TGF-β, thereby mitigating SiNPs-induced lung injury.

Conclusion Exposure to SiNPs may cause pulmonary inflammation and fibrotic injury through NETs/integrins/TGF-β and NETs/cytokines/CD44 signaling pathways. Targeting NETs degradation may offer a novel therapeutic target for SiNPs-induced lung injury and provide a potential therapeutic avenue for inflammatory and fibrotic related diseases.

†Xiu He, Xiaoli Yuan and Xuedong Sa contributed equally to this work.

*Correspondence:
Xiu He
hexiu@gmc.edu.cn
Jun Li
gygwlj@163.com

Full list of author information is available at the end of the article

Keywords Silica nanoparticles, Pulmonary injury, Neutrophil extracellular traps, Bioinformatic analysis

Graphical Abstract

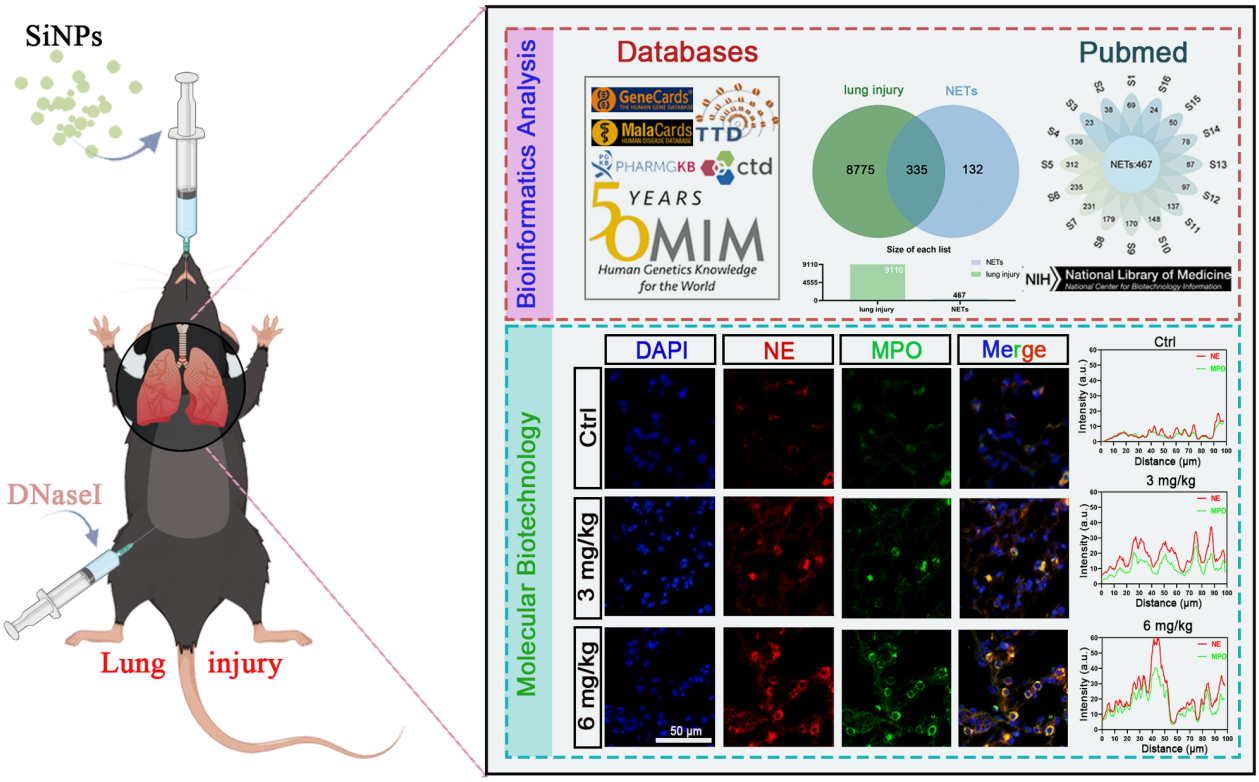

Background

Nanoparticles are defined as materials with having at least one physical dimensional diameter is larger than 1 nm, but less than 100 nm. According to the latest research report from Technavio, the global nanotechnology products market size is projected to expand by USD 161.3 billion from 2024 to 2028, exhibiting a Compound Average Growth Rate (CAGR) of 18.53% [1]. The mass production and widespread use of nanomaterials in everyday products have raised concerns regarding their safety [2, 3]. Silica nanoparticles (SiNPs) represent the second most abundant nanomaterials in the global market, with an annual production volume approaching 1.5 million tonnes. Continued growth in global manufacturing is anticipated to meet market demand [4]. According to a Global Information report, the global nano silica market was valued at $3.52 billion in 2021 (https://www.giiresearch.com/) [5]. SiNPs have a wide range of app lication across various fields, such as chemical industry, food, cosmetic, biomedicine, rubber, paints, electronics, etc. According to SPER Market Research, the global nano silica market is estimated to reach USD 7.90 billion by 2030 with a CAGR of 6.2% (https://www.giiresearch.com/). Humans are routinely exposed to SiNPs in non-occupational and occupational environments, and these exposures have the potential to induce adverse health effects. Although numerous studies have shown that exposure to SiNPs can adversely affect multiple organs and organ systems, such as the brain, liver, kidney, and cardiovascular and respiratory systems, the mechanism of its toxic action remains incompletely understood [4, 6–9]. Current research on SiNPs mainly focuses on the application of nanotechnology, while the toxicological evaluation of nanoparticles lags significantly behind their applications. SiNPs have been listed in the priority nanomaterials for toxicity assessment by Organization for Economic Co-operation and Development (OECD) [4]. Inhalation is one of the most significant exposure pathways for SiNPs in industries such as nanomaterials production, coal mining and construction [10]. Studies have demonstrated that inhalation of SiNPs can lead to the occurrence of pulmonary inflammation and fibrosis [9, 11, 12]. Despite extensive research, the exact mechanism of SiNPs-induced lung damage remains unclear.

Neutrophils are the most abundant peripheral immune cells in circulation and serve as the first line of innate immune defense against infections and tissue injury. They are associated with various pathophysiological

conditions, including autoimmune diseases, chronic inflammatory diseases, cancer, and tissue repair, through mechanisms such as degranulation, phagocytosis, and the release of neutrophil extracellular traps (NETs) [13, 14]. NETs are reticular complexes composed of double-stranded DNA, decorated with various proteins including neutrophil elastase (NE), cathepsin G (CG), myeloperoxidase (MPO), matrix metalloproteinase 9 (MMP9), citrullinated histone H3 (CitH3), and protein-arginine deiminase type 4 (PAD4), etc [15]. Activated neutrophils release NETs, which exhibit antimicrobial activity. However, excessive NET production has been correlated with inflammation, fibrosis, and tissue damage. Studies have shown that NETs contribute to inflammatory injury in cases of acute lung injury (ALI) [16–18]. Patients with severe asthma exhibit increased levels of NETs components in sputum. Furthermore, DNase I, an inhibitor of NETs, prevents NETs-induced inflammasome activation and IL-1β secretion in airway epithelial cells [19]. Recent studies have shown that NETs contribute to the development of chronic obstructive pulmonary disease (COPD) and are involved in virus-induced COPD exacerbations [20, 21]. Additionally, NETs also have been identified as playing a crucial role in crystal-associated diseases [22]. Although a recent study [23] links NETs to acute pulmonary inflammation after short-term, high-dose exposure to SiNPs, real-world occupational exposure is typically chronic, occurs at relatively low levels, and often leads to more severe progressive fibrosis. Whether NETs contribute to the inflammatory and fibrotic responses induced by long-term, occupational-level SiNPs exposure, and the underlying mechanisms, remains unclear.

Integrins are a kind of cell adhesion receptor superfamily, which are heterodimers consisting of two chains, α and β [24]. Integrins are essential for regulating fundamental physiological processes, including inflammation, immune response and wound healing [25]. Virtually all cells express a contingent of integrins; in vertebrates, 24 distinct αβ heterodimers have been identified, with the β2 family are specifically expressed on leukocytes [24]. Four distinct integrin β2 families are expressed on neutrophils, including αLβ2 (LFA-1, CD11a/CD18), αMβ2 (Mac-1, CR3, CD11b/CD18), αXβ2 (CR4, CD11c/CD18) and, αDβ2 (CD11d/CD18) [26]. Raftery et al. showed that hantavirus induces kidney and lung damage through the αMβ2-mediated release of NETs [27]. Integrins have also been implicated in promoting pulmonary fibrosis by regulating the formation of NETs in fibrotic interstitial lung disease (ILD) [28]. Moreover, studies indicate that integrins can also be regulated by NETs and engage in various pathological processes. NETs induce a TGF-β-dependent epithelial-mesenchymal transition (EMT) in cancer cells. Pharmacological targeting of the NETs/αvβ1/MMP9/TGF-β axis has been shown to enhance chemotherapy efficacy [29]. Laminin remodeled by NETs formed during lung inflammation activates integrin a3β1, which in turn awakens dormant cancer cells in mice [30]. Overall, while NETs and integrins can modulate one another and facilitate disease progression, it is still unclear whether and how NETs and integrins contribute to SiNPs-induced lung injury.

To address this gap, we constructed a mouse model of occupational SiNPs exposure to assess SiNPs-induced pulmonary inflammation and fibrosis. Subsequently, we employed bioinformatics and molecular biotechnology to comprehensively predict and evaluate the alterations of NETs and integrins involved in SiNPs-induced pulmonary injury. Additionally, using the NETs inhibitor DNase I, we examined whether SiNPs-induced NETs, integrins and lung injury could be regulated. Our conclusions may help to identify new molecular mechanisms and specific molecular targets of lung injury induced by occupational exposure to SiNPs from the perspective of NETs.

Materials and methods

Chemicals and reagents

The SiNPs utilized in this study were obtained from Nanocomposix (USA) (80 nm, 10 mg/mL, SIAN80-25mL). DNase I (04536282001) was purchased from Sigma (Sigma Aldrich, USA). The Western Blot Kit was purchased from Changzhou Smart-Lifesciences Biotechnology Co (China). The following primary antibodies were used in this study: anti-αM (ab128797) and anti-CitH3 (ab281584) was purchased from Abcam (Cambridge, MA, USA); anti-αL (abs115674), anti-IL-18 (abs120003) ,and anti-IL-6 (abs135607) were purchased from Absin Corporation (Shanghai, China); anti-β2 (10554-1-AP), anti-Col1 (14695-1-AP), anti-TGF-β (21898-1-AP), anti-PAD4 (17373-1-AP), anti-Fn1 (15613-1-AP), anti-MPO (10375-1-AP), anti-MMP9 (10375-1-AP), anti-α-SMA (14395-1-AP), goat anti-rabbit IgG H&L (FITC, SA00003-2) and goat anti-mouse IgG H&L (TRITC, SA00007-1) were purchased from Proteintech Group, Inc. (Chicago, USA); anti-IL-1β (sc-52012), anti-CD44 (sc-7297), anti-LY6G (sc-53515), and anti-NE (sc-514720) were purchased from Santa Cruz Biotechnology Inc. (Dallas, TX, USA); anti-β-actin (13E5) rabbit antibody was obtained from Cell Signaling Technology, Inc. (Boston, USA). Alexa Fluor® 488-AffiniPure Fab Fragment Goat Anti-Rabbit IgG (H + L) was obtained from Jackson ImmunoResearch Laboratories, Inc. (111-547-003, West Grove, Pennsylvania, USA).

Characterization of SiNPs

The morphology of the SiNPs was characterized using Transmission Electron Microscopy (TEM). The average particle diameter was determined through Image J software. The SiNPs suspension was sonicated for 30 min

until a homogeneous dispersion was achieved. The hydrodynamic size and Zeta potential of the SiNPs in saline were measured by Zetasizer (Malvern NanoZS90, UK).

Animals and treatment

Healthy male C57BL/6 mice (20 ± 2 g, 6–8 weeks old) were purchased from the Experimental Animal Research Center at Guizhou Medical University (Guiyang, China) [Certificate number SYXK (Gui) 2023-0002]. All efforts were made to minimize the number of animals used and their suffering. The mice were provided with standard rodent chow and had unrestricted access to pure water. Prior to the experiment, all animals were acclimatized for a period of one week. All experiments were conducted in accordance with the guidelines of Guizhou Medical University for the care and use of laboratory animals and were approved by the Animal Ethical Committee of Guizhou Medical University [Number 2100247].

Study 1: After a 7-day acclimatization period, Male C57BL/6 mice were randomly divided into 3 groups, each containing 10 mice: the control group (Ctrl) and two SiNPs groups administered at doses of 3.0 (3 mg/kg) and 6.0 mg/kg·bw (6 mg/kg), respectively. The exposure method, dose, and duration were selected based on published studies [31] and our group's prior work [32] to simulate the actual exposure conditions. Briefly, mice in the 3 mg/kg and 6 mg/kg SiNPs groups were anesthetized with chlorpromazine and received intratracheal instillations of SiNPs suspension (45 ± 5 μL) once weekly for a total of 12 administrations; the control group received equivalent volumes of 0.9% saline.

Study 2: To investigate the role of NETs in SiNPs-induced lung injury, C57BL/6 mice were randomly divided into 4 groups: Control group (Ctrl), 6 mg/kg SiNPs group (SiNPs), DNase I reagent control group (DNase I), and DNase I + SiNPs group. DNase I (300 U per mouse) was administered intraperitoneally three times per week for 12 weeks. The dose was selected based on Mousset et al. [29]. To minimize adverse effects from daily handling and injections and guided by our group's experience with silicosis animal-model interventions [33, 34], the dosing regimen comprised an injection given before SiNPs exposure on the first day of each week, followed by additional injections on days 3 and 5.

Bronchoalveolar lavage fluid (BALF) collection and inflammatory cytokines analysis

BALF was collected as previously described [35]. Briefly, lung tissues were lavaged twice with 1mL of pre-cooled sterile saline. The BALF was then centrifuged at 800 rpm at 4℃ for 10 min, and the supernatant was extracted and transferred to new centrifuge tubes, which were subsequently stored at -80℃ for the detection of inflammatory cytokines. Cytokine assays were performed using a Bio-Plex Pro Mouse Chemokine kit (Bio-Rad). Multiplex levels of inflammatory biomarkers were measured using the MSD Platform (labservice.univ-bio.com, Shanghai, China). The Luminex multiplex cytokine assay was employed to detect inflammatory cytokines in the BALF of each group, performed by LabEx (Shanghai, China) using the Luminex X-200 (Luminex). Instrument operation and data acquisition procedures were conducted by Univ-Bio.

Histological staining analysis

Paraffin-embedded lung tissues were cut into 5 μm slices and mounted on anti-slip slides. Hematoxylin & Eosin (H&E) and Masson's trichrome staining were performed to evaluate lung inflammation and fibrosis. For H&E staining, lung slices were stained with hematoxylin for 5 min and eosin for 3 min. For Masson's trichrome staining, sections were stained with hematoxylin for 1 min, acid fuchsin stain solution for 5 min, differentiation solution for 30 s, and aniline blue counterstain for 1 min. Histological sections were sealed with neutral gum and then observed and photographed using a digital slide scanner (NanozoomerS60, Hamamatsu, Japan). The inflammatory and fibrotic scores of the lung sections were evaluated according to the criteria established by Mikawa et al. [36] and Hubner et al. [37].

Bioinformatics data collection and analysis

Targets associated with lung injury were collected from the Online Mendelian Inheritance in Man (OMIM, https://omim.org/), GeneCards (https://www.genecards.org/), the Therapeutic Targets Database (TTD, https://db.idrblab.org/ttd), the Comparative Toxicogenomics Dat abase (CTD, http://ctdbase.org/), MalaCards (https://www.malacards.org/), and the PharmGKB platform (https://www.pharmgkb.org/). All collected lung injury targets were converted into target IDs in the UniProt database (https://www.uniprot.org/). The six databases were merged and de-weighted. The acquisition of NET-related genes (NRGs) was based upon the integration of pertinent gene sets from the relevant NRGs literature within the PubMed literature database, in accordance with the preceding research methodologies [38, 39].

The data pertaining to lung injury and NRGs targets were imported into the Venn plugin of the bioinformatics platform (http://www.bioinformatics.com.cn/static/others/jvenn/example.html) for analysis. The overlapped genes were integrated into the protein-protein interaction (PPI) network using the STRING database (https://cn.string-db.org/), with the organism restricted to "Homo sapiens" with a minimum required interaction score of ≥ 0.9. The resulting network was visualized by Cytoscape 3.10.2 software (National Institute of General Medical Sciences,

Boston, MA, USA). CytoNCA was employed to identify pivotal genes with the top values of degree centrality, betweenness centrality, and closeness centrality. Only genes exceeding the median values of these three indicators were considered key gene targets.

The targets were analyzed using DAVID (https://david.ncifcrf.gov/summary.jsp) for GO function and KEGG pathways enrichment. P-values were obtained from the DAVID database and filtered to be below 0.05. The top 20 ranked terms were subjected to further enrichment analysis. The primary biological processes, cellular components, molecular functions, and KEGG pathways of the genes were further enriched using the Metascape platform (https://metascape.org/gp/index.html). The results were visualized using a bioinformatics website (http://www.bioinformatics.com.cn/).

Immunofluorescence

Paraffin-embedded lung tissue Sect. (5 μm) were deparaffinized and washed three times with PBS for 5 min each time. Nonspecific binding sites in the lung tissue sections were blocked using 10% donkey serum albumin. The sections were then incubated overnight at 4 °C with anti-LY6G (1:100) and anti-CitH3 (1:500), anti-NE (1:100) and anti-MPO (1:100), anti-αM (1:100) and anti-β2 (1:100), anti-αL (1:100) and anti-β2 (1:100). Subsequently, the goat anti-rabbit FITC (1:50), anti-mouse TRITC secondary antibody (1:50) mixture were added and incubated at a room temperature for 2 h. Finally, the slices were washed 3 times for 10 min and mounted with ProLong® Diamond Antifade Mountant containing DAPI. Images were captured using a fluorescence microscope (Nikon, Tokyo, Japan) under consistent conditions. The fluorescence intensity was analyzed using the Image J software.

TEM of lung tissue

The lung tissue was pre-fixed in a 3% glutaraldehyde solution, followed by re-fixed with 1% osmium tetroxide. Subsequently, the tissue samples were dehydrated through acetone gradients and embedded in resin. Ultrathin sections, 50 nm in thickness, were then prepared using a Leica EM UC7 ultramicrotome (Leica Biosystems, Vista, CA, USA) and stained with uranyl acetate and lead citrate. The slices were subsequently observed and imaged using TEM (JEOL Company, Tokyo, Japan).

Western blotting

Lung tissues were lysed with radio immunoprecipitation assay buffer (RIPA) containing phenylmethylsulfonyl fluoride (PMSF). The resulting lysate centrifuged at 10,000 rpm for 10 min at 4 °C, and the supernatant was collected. Protein concentration was quantified according to the bicinchoninic acid (BCA) protein assay kit. Subsequently, 5X protein loading buffer was added to adjust the protein concentration to 3 μg/μL. The protein samples were denatured at 100℃ for 5 min, cooled to room temperature, and either immediately used for sodium dodecyl sulfate polyacrylamide gel electrophoresis (SDS-PAGE) or stored at -80℃. For SDS-PAGE, 30 μg of protein samples were separated on the gels and subsequently transferred onto polyvinylidene fluoride (PVDF) membranes (Millipore, Billerica, MA, Germany). After a 1-hour incubation with 5% bovine serum albumin (BSA), the membranes were incubated at 4 °C with primary antibodies, including anti-CD44 (1:400), anti-αL (1:2000), anti-IL-1β (1:1000), anti-IL-6 (1:3000), anti-IL-18 (1:3000), anti-αM (1:5000), anti-β2 (1:2000), anti-MMP9 (1:3000), anti-MPO (1:300), anti-PAD4 (1:3000), anti-Col1 (1:3000), anti-Fn1 (1:3000), anti-TGF-β (1:3000), anti-α-SMA (1:3000), and anti-β-actin (1:3000). The membranes were then washed three times with 1×tris-buffered saline with Tween-20 (TBST) and incubated for 2 h at room temperature with corresponding HRP-conjugated secondary antibodies (1:5000). Finally, the blots were detected using the Easy Enhanced Chemiluminescence Western Blot Kit, and the specific protein was visualized with an imaging system (Bio-Rad Laboratories Inc., Hercules, USA). The optical density was determined using Image J software (National Institutes of Health, Bethesda, MD).

Statistical analysis

All figures in this study were generated using GraphPad Prism 9.5. The data are presented as mean ± standard deviation (*SD*) and were analyzed using SPSS version 25.0 (IBM Corp, USA). Comparisons among groups exceeding two were conducted using one-way analysis of variance (*ANOVA*). A probability value of less than 0.05 ($P < 0.05$) was considered statistically significant in all cases.

Results

Characterization of SiNPs

As shown in Fig. 1A, SiNPs exhibited generally near-spherical shape with a relatively well dispersion. The average diameter of SiNPs was 78.200 nm. Their hydrodynamic size and zeta potential in saline were present in Fig. 1B; Table 1.

Exposure to SiNPs induces pulmonary injury in C57BL/6 mice

A murine model was established to investigate the impact of SiNPs on the lung tissues. The modelling process was illustrated in Fig. 2A. Compared to the Ctrl group, the weight of mice in 6 mg/kg group was significantly reduced ($P < 0.05$) (Fig. 2B). H&E and Masson's trichrome staining were employed to demonstrate the injury effect of SiNPs on lung tissues. The H&E staining results in Fig. 2C&D showed inflammatory cell infiltration in the

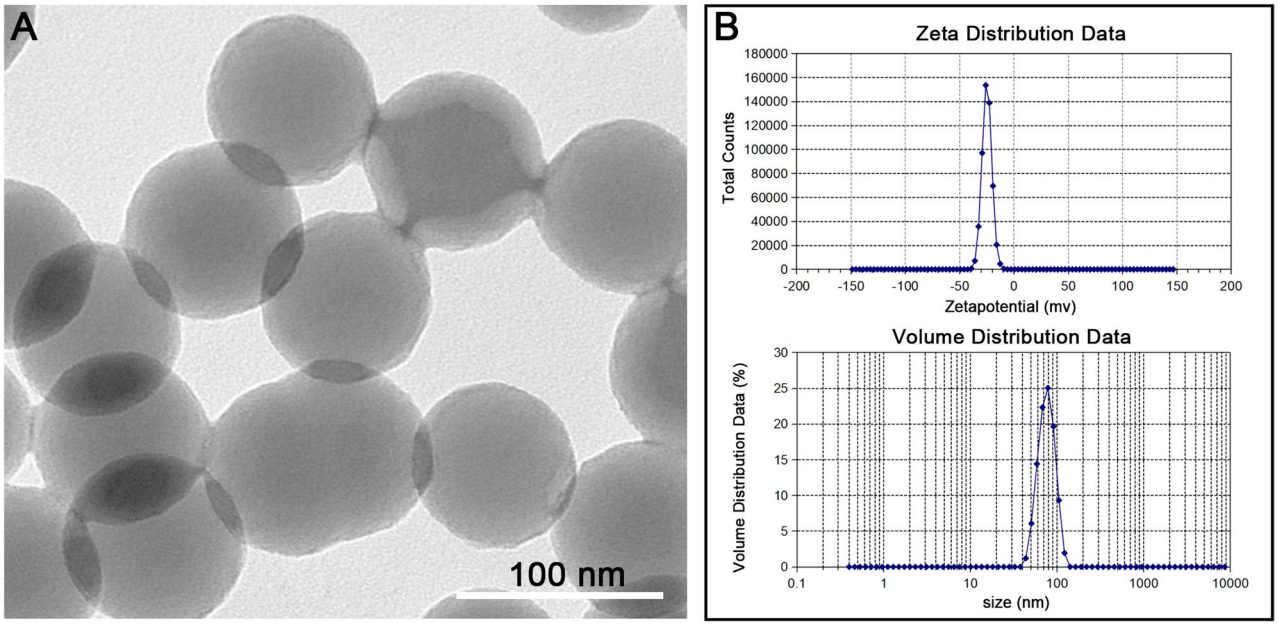

Fig. 1 Characterization of SiNPs. (**A**) TEM images of SiNPs, scale bar = 100 nm. (**B**) Distribution of hydrodynamic size and zeta potential of SiNPs in saline

Table 1 Characterization of SiNPs

Characteristic	SiNPs
Hydrodynamic size (nm) (mean ± *SD*)	78.200 ± 2.202
Zeta Potential (mV) (mean ± *SD*)	-24.963 ± 0.005
Morphology	Spheroid
Aggregation	Absent
Crystalline structure	Amorphous

lungs of mice from the 6 mg/kg SiNPs group. As depicted in Fig. 2E&F, collagen deposition was observed in the lung tissues of mice from the 3 mg/kg and 6 mg/kg SiNPs groups.

Bioinformatics analysis identify genes and pathways associated with NETs in lung injury

A total of 149,609 human lung injury-related genes were collected from several databases, including GeneCards, MalaCards, OMIM, ParmGKB, TTD and CTD (detailed information is illustrated in Table S1, Fig. S1A and Fig. 3A). Genes from six databases were combined and de-weighted, resulting in 9,110 genes identified as relevant to lung injury (Table S1 and Fig. 3B). Additionally, sets of genes associated with NETs were collected from the PubMed database for the period from October 2019 to October 2024 (detailed information is provided in Table S2). A total of 467 NETs-related genes were obtained by combining 16 gene sets (Fig. 3C). We then identified the overlapping genes between the aforementioned lung injury-related genes and NETs-related genes, yielding 335 intersecting targets (Fig. 3D). Subsequently, these 335 genes were input into the STRING database with a minimum required interaction score of ≥ 0.9 to create a protein-protein interaction (PPI) network, which was visualized by Cytoscape (Fig. S1B-C). The CytoNCA plugin was employed to calculate the Degree Centrality (DC), Betweenness Centrality (BC), and Close to Centrality (CC) values above the median, which was used as the cut-off point to identify the centermost 96 core target genes in Fig. 3E. Notable core targets include MMP9, integrin subunits αM (ITGAM), integrin subunits β2 (ITGB2), CD44, TGF-β, interleukin-6 (IL-6), IL-1β, CXCL1, IL-10 and FN (Fn1), among others. To further elucidate the biological functions of the identified 96 target genes, Gene Ontology (GO) and Kyoto Encyclopedia of Genes and Genomes (KEGG) analyses were performed using the DAVID 6.8 database, with a significance threshold of $P < 0.05$. The top 20 terms with the lowest P values in biological processes (BP), cellular components (CC), and molecular functions (MF) were selected and visually depicted in the enrichment analysis diagram (Fig. 3F-J, Fig. S1D-E). The results of KEGG, MF, CC and BP showed that NETs formation, integrin family, inflammatory response, chemokine activity, TNF-α pathway and cellular response to interleukin were associated with NETs in lung injury.

Exposure to SiNPs induces pulmonary inflammation and fibrosis in C57BL/6 mice

The results of Luminex multifactor analysis presented in Fig. 4A indicated that levels of IL-1β, CCL12, IL-6, CCL24, CXCL1, CX3CL1, CCL27, CXCL10, IL-2, TNF-α, IFN-γ, MCP-1, CCL1, and MIP-1α were increased, while IL-10 levels were decreased in the BALF of the SiNPs-exposed groups. These findings suggested the

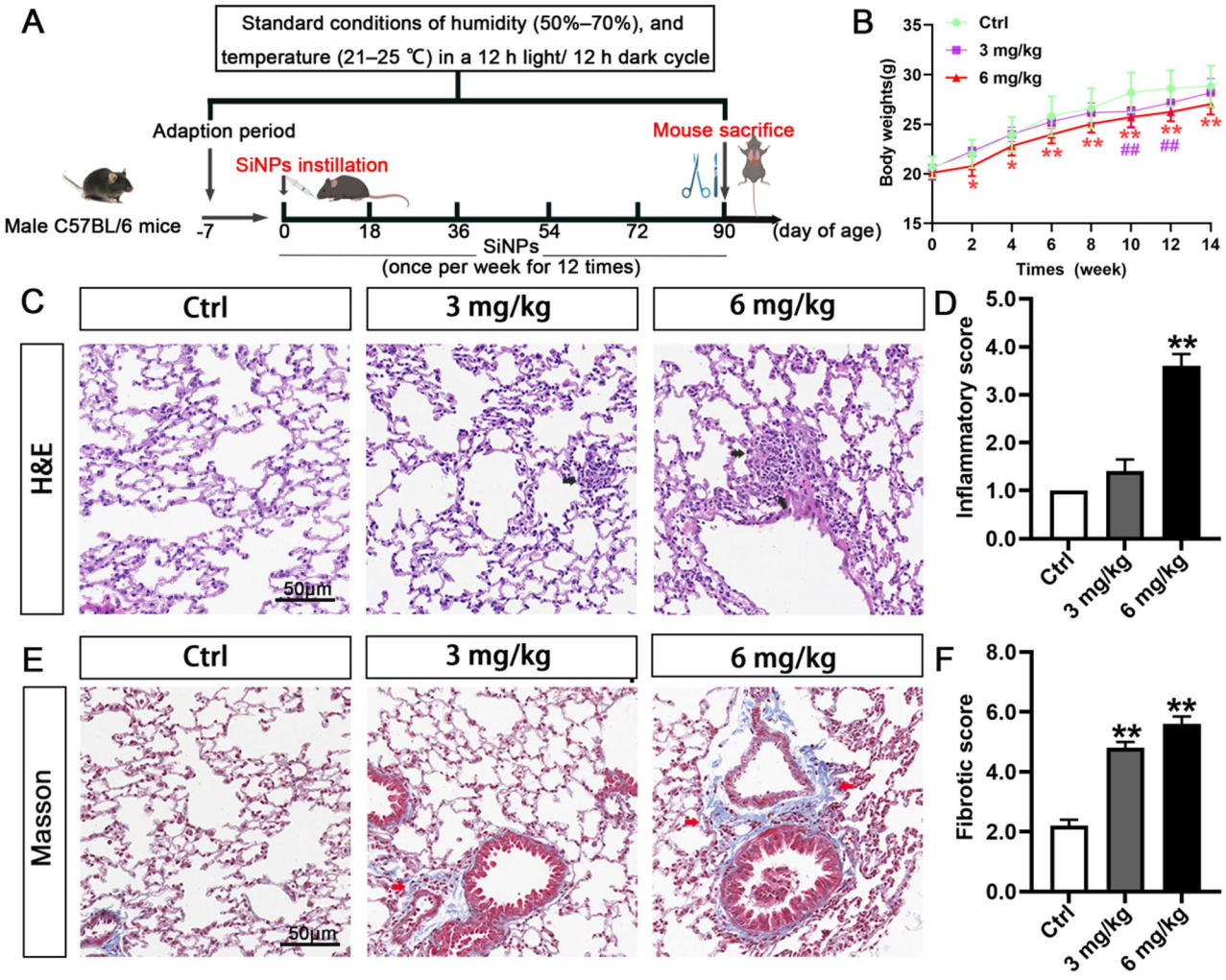

Fig. 2 Exposure to SiNPs induces lung injury in C57BL/6 mice. (**A**) Schematic diagram illustrating the SiNPs exposure model. (**B**) Body weight measurements during the experiment periods ($n = 10$), * $P < 0.05$, ** $P < 0.01$, 6 mg/kg group vs. Ctrl group; ## $P < 0.01$, 3 mg/kg group vs. Ctrl group. (**C**) H&E staining of mice lungs (black arrows: inflammatory cell infiltration, scale bar = 50 μm). (**D**) Inflammatory score analysis of lung sections ($n = 5$). (**E**) Masson's trichrome staining of mice lungs (red arrows: collagen deposition, scale bar = 50 μm). (**F**) Fibrotic score analysis of lung sections ($n = 5$). Data are presented as the mean ± *SD*. * $P < 0.05$, ** $P < 0.01$, vs. Ctrl group

potential presence of inflammatory injuries in lung tissues. To further clarify the changes in lung tissue inflammation and fibrosis indexes, we employed Western blotting analysis. The results shown in Fig. 4B-E demonstrated that exposure to 6 mg/kg SiNPs significantly elevated the expression of inflammatory factors, including IL-1β, IL-6, and IL-18 in lung tissues. Additionally, as illustrated in Fig. 4F-I, a notable elevation in fibrosis indexes Fn1, Col1, and α-SMA was observed in the lung tissues of the 6 mg/kg SiNPs group. Collectively, these data reveal that inhalation exposure to SiNPs induces pulmonary inflammation and fibrosis in mice.

Effect of SiNPs exposure on NETs in C57BL/6 mice

The bioinformatics analysis results indicated that the formation of NETs was linked to lung injury, although the role of NETs in SiNPs-induced lung injury is still unclear. Consequently, we comprehensively evaluated the expression of NETs in the lung tissues of SiNPs-exposed mice using TEM, Western blotting and immunofluorescence staining techniques. As depicted in Fig. 5A, neutrophils in the Ctrl group were structurally intact and morphologically normal, whereas in the SiNPs-exposed group, the plasma membrane was disrupted, and extracellular release was increased. Western blotting analysis revealed that the expression levels of NETs-related proteins MMP9, PAD4, and MPO were elevated in the 6 mg/kg SiNPs group ($P < 0.05$, Fig. 5B-E). Immunofluorescence single stain results also showed increased expression of MMP9 and PAD4 (Fig. S2A-E). Co-staining using

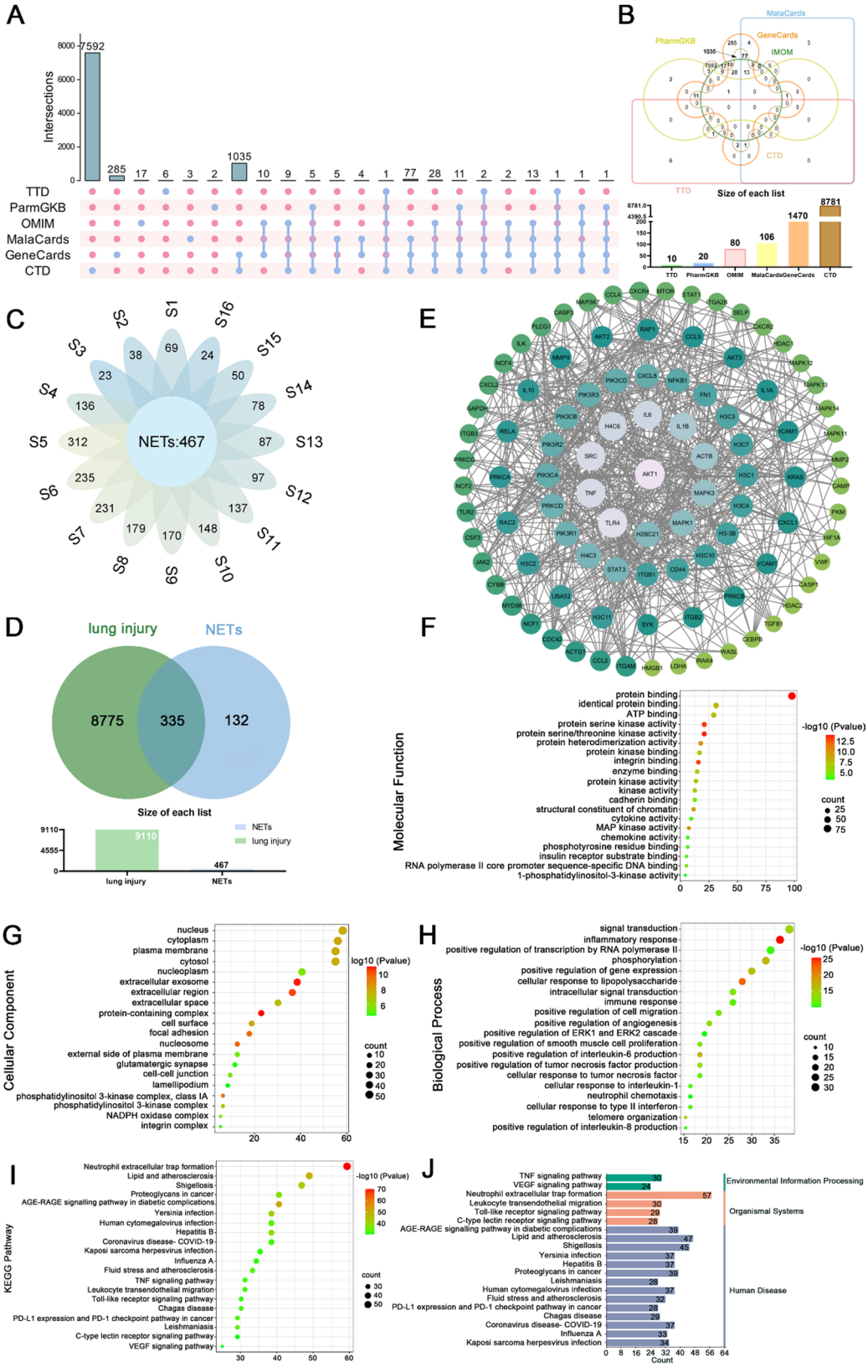

Fig. 3 (See legend on next page.)

(See figure on previous page.)

Fig. 3 Bioinformatics analysis identify genes and pathways associated with NETs in lung injury. (**A**) The relationship of overlapping and independent sets of genes between the lung injury-associated gene databases in the upset plot. Vertical histogram represents number of genes in each subset. Pink dots denote "not included" and blue dots denote "included." Connected dots in the same column indicate that the corresponding blue-dot sets constitute the intersection of that column. (**B**) The lung injury-associated targets were obtained based on CTD, TTD, OMIM, PharmGKB, GeneCards and MalaCards database. (**C**) The flower plot of 16 NETs-related genes set retrieved from the PubMed database. (**D**) Venn diagrams of NETs-related gene targets and lung injury targets. (**E**) The hub genes were selected from the PPI network using the CytoNCA plugin. (**F-H**) The bubble diagram of the first 20 entries in the GO analysis of lung injury-related target genes associated with NETs. (**I-J**) The bubble plots and categorical histograms of the top 20 pathways based on KEGG enrichment analysis

LY6G (a specific marker for neutrophils) and CitH3, NE and MPO demonstrated that the intensity and co-localization of the red and green fluorescence were significantly enhanced in the 6 mg/kg SiNPs group (Fig. 5F-I). Together, these results suggest that exposure to SiNPs increases the production of NETs, which may contribute to SiNPs-induced lung injury.

Integrins, CD44 and TGF-β are involved in SiNPs-induced lung injury

Integrins have important physiological functions, and studies have reciprocal regulatory relationship between integrins and NETs. The β2 integrins family, which are specifically expressed on leukocytes, are implicated in lung injury, as suggested by the bioinformatics analyses shown in Fig. 3E-G. To further investigate the role of integrins in SiNPs-induced lung injury, Western blotting and immunofluorescence were used to assess the changes in protein levels of integrin subunits αL, αM and β2. As shown in Fig. 6A-D, the protein levels of integrin subunits αL, αM and β2 were significantly increased in 6 mg/kg SiNPs group ($P<0.01$). Additionally, immunofluorescence analysis of αL and β2, as well as αM and β2, revealed a significant increase in fluorescence intensity and colocalization in the SiNPs group (Fig. 6G-H). These results indicate the potential involvement of integrins αLβ2 and αMβ2 in SiNPs-induced lung injury. CD44 and TGF-β are known to play crucial roles in respiratory diseases. Bioinformatics analysis further predicted that CD44 and TGF-β may be associated with NETs and lung injury. Immunofluorescence staining revealed that the intensity of the red CD44 fluorescence was significantly enhanced in the SiNPs group (Fig. S2E&F). Additionally, Western blotting results showed a significant increase in CD44 and TGF-β protein levels in the 6 mg/kg SiNPs group compared to the Ctrl group ($P<0.05$) (Fig. 6I-K).

DNase I reduces SiNPs-induced NETs and inhibits the expression of integrins, CD44 and TGF-β

To elucidate the role of NETs, integrins, CD44 and TGF-β in SiNPs-induced lung injury, DNase I was employed to intervene in SiNPs-exposed mice (Fig. S3A). As demonstrated by the TEM results in Fig. 7A, the plasma membrane of neutrophils was disrupted, and extracellular release was increased in the SiNPs-exposed group. DNase I effectively alleviated the neutrophil damage induced by SiNPs. Western blotting analysis revealed that DNase I significantly mitigated SiNPs-induced elevations of the NETs-associated proteins MPO, PAD4, and MMP9 ($P<0.05$, Fig. 7B-E). Immunofluorescence single-staining results also indicated that DNase I significantly mitigated SiNPs-induced elevations of MMP9 and PAD4 (Fig. S4A-D). Immunofluorescence co-staining with LY6G and CitH3, and with NE and MPO, demonstrated that the intensity and co-localization of red and green fluorescence enhanced by SiNPs were restrained by DNase I (Fig. 7F-I). To elucidate the regulatory relationship between NETs and related indicators, we subsequently evaluated the expression of integrins and CD44. Compared to the SiNPs group, the levels of integrin subunits αM, αL, and β2 were significantly reduced in the DNase I + SiNPs group ($P<0.05$, Fig. 7J-M). Immunofluorescence staining demonstrated that the enhancement of red CD44 fluorescence induced by SiNPs was mitigated by DNase I (Fig. S3E&F). Additionally, measurement of CD44 and TGF-β in lung tissues revealed that the protein levels were lower in DNase I + SiNPs group than in the SiNPs group ($P<0.05$, Fig. 7N-P). These findings suggest that NETs exert regulatory effects on integrins, CD44, and TGF-β in the mouse model of SiNPs-induced lung injury.

Inhibition of NETs effectively alleviate SiNPs-induced lung injury

Mice in the SiNPs group exhibited a significant reduction in body weight (bw), while DNase I treatment did not exert a notable mitigating effect on SiNPs-induced weight loss (Fig S3B). The results from Luminex multifactor detection, as illustrated in Fig. 8A, indicated that DNase Ⅰ inhibited the SiNPs-induced increases in levels of IL-1β, CCL12, IL-6, CCL24, CXCL1, CX3CL1, CCL27, CXCL10, IL-2, TNF-α, IFN-γ, MCP-1, CCL1, and MIP-1α in BALF, while reversing the decrease in IL-10 levels. These findings suggest that the inhibition of NETs may attenuate SiNPs-induced inflammatory injury. Therefore, we subsequently conducted Western blotting, H&E and Masson's trichrome staining of lung tissue to assess whether DNase Ⅰ could attenuate SiNPs-induced lung injury. The results illustrated in Fig. 8B-E showed that the protein levels of IL-6, IL-1β and IL-18 were significantly lower in the DNase I + SiNPs group compared to the SiNPs group ($P<0.05$). H&E staining further

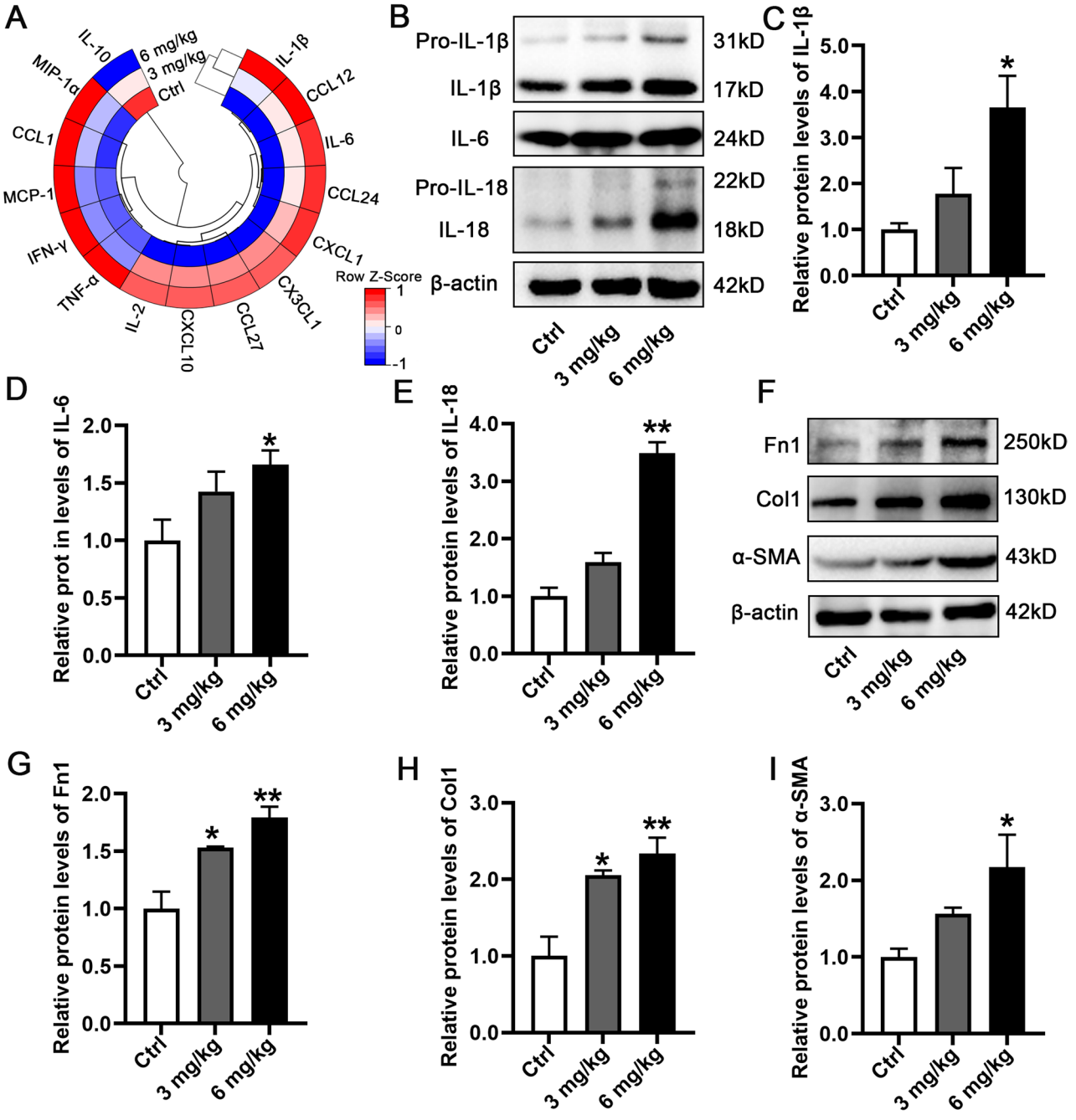

Fig. 4 Exposure to SiNPs induces pulmonary inflammation and fibrosis in C57BL/6 mice. (**A**) Luminex multifactor detection of cytokines in BALF across all groups. The heatmap shows clustering based on average linkage performed by Origin's Polar Heatmapper Dendrogram plugin [40]. The Z-Score indicates the deviation from the average level of the marker across groups, higher Z-scores are indicated in red and lower Z-scores in blue. 0 represents the cytokine's mean expression across groups, while + 1/−1 indicate one standard deviation above/below the mean, respectively. (**B-E**) Western blotting analysis of IL-1β, IL-6 and IL-18 protein levels in lung tissues ($n = 3$). (F-I) Western blotting analysis of Fn1, Col1 and α-SMA protein levels in lung tissues ($n = 3$). Data are expressed as the mean ± *SD*. * $P < 0.05$, ** $P < 0.01$, vs. Ctrl group

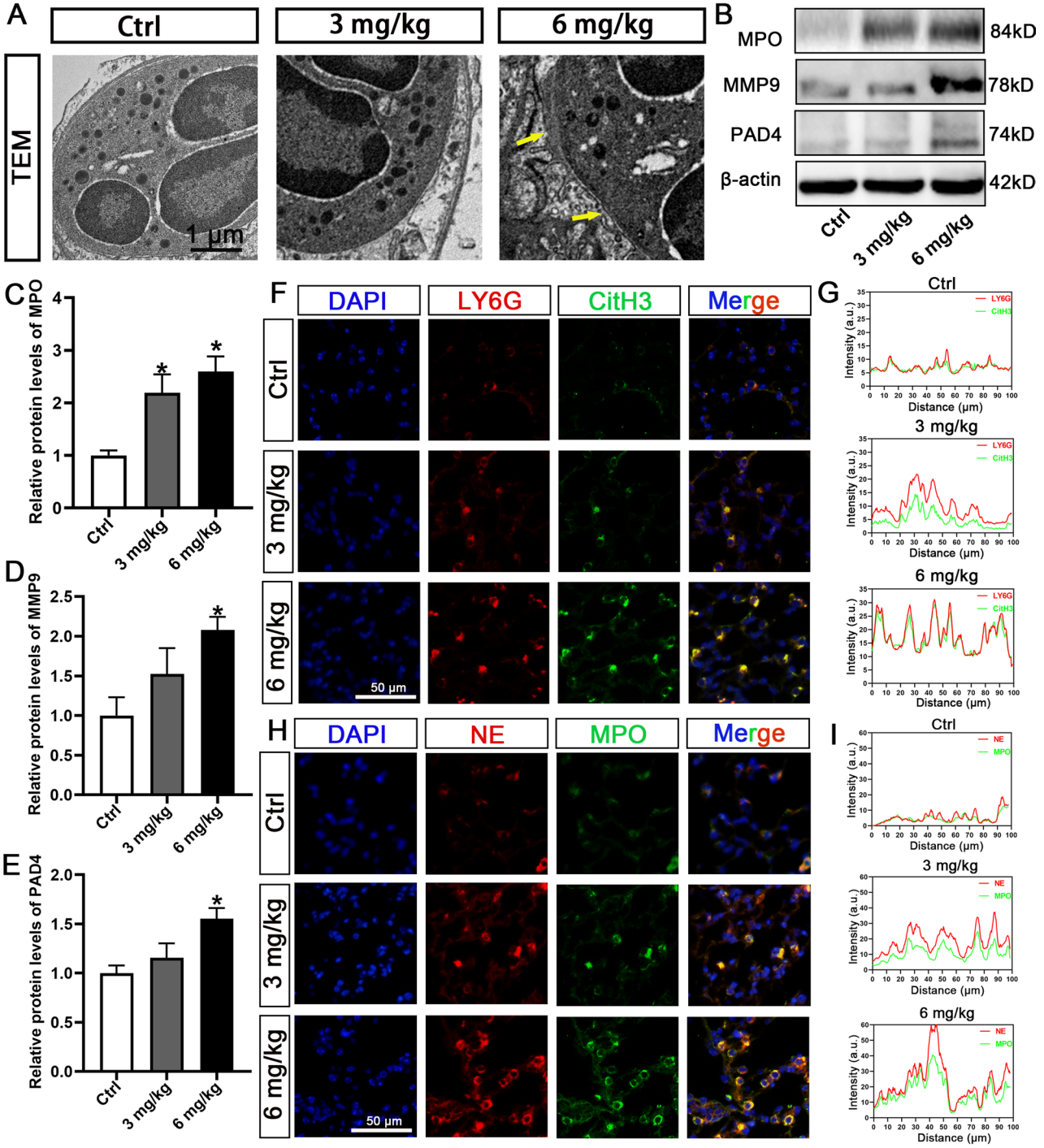

Fig. 5 Effect of SiNPs exposure on NETs in C57BL/6 mice. (**A**) TEM of lung tissue (yellow arrows: the disrupted cell membrane, scale bar = 1 μm). (**B-E**) Western blotting analysis of MPO, MMP9, and PAD4 protein levels in lung tissues ($n = 3$). (**F**) Immunofluorescence staining for CitH3 and LY6G in lung tissue (scale bar = 50 μm). (**G**) Immunofluorescence staining for MPO and NE in lung tissue (scale bar = 50 μm). (**H-I**) Analysis of the colocalization of the red and green fluorescence. Data are expressed as the mean ± *SD*. * $P < 0.05$, vs. Ctrl group

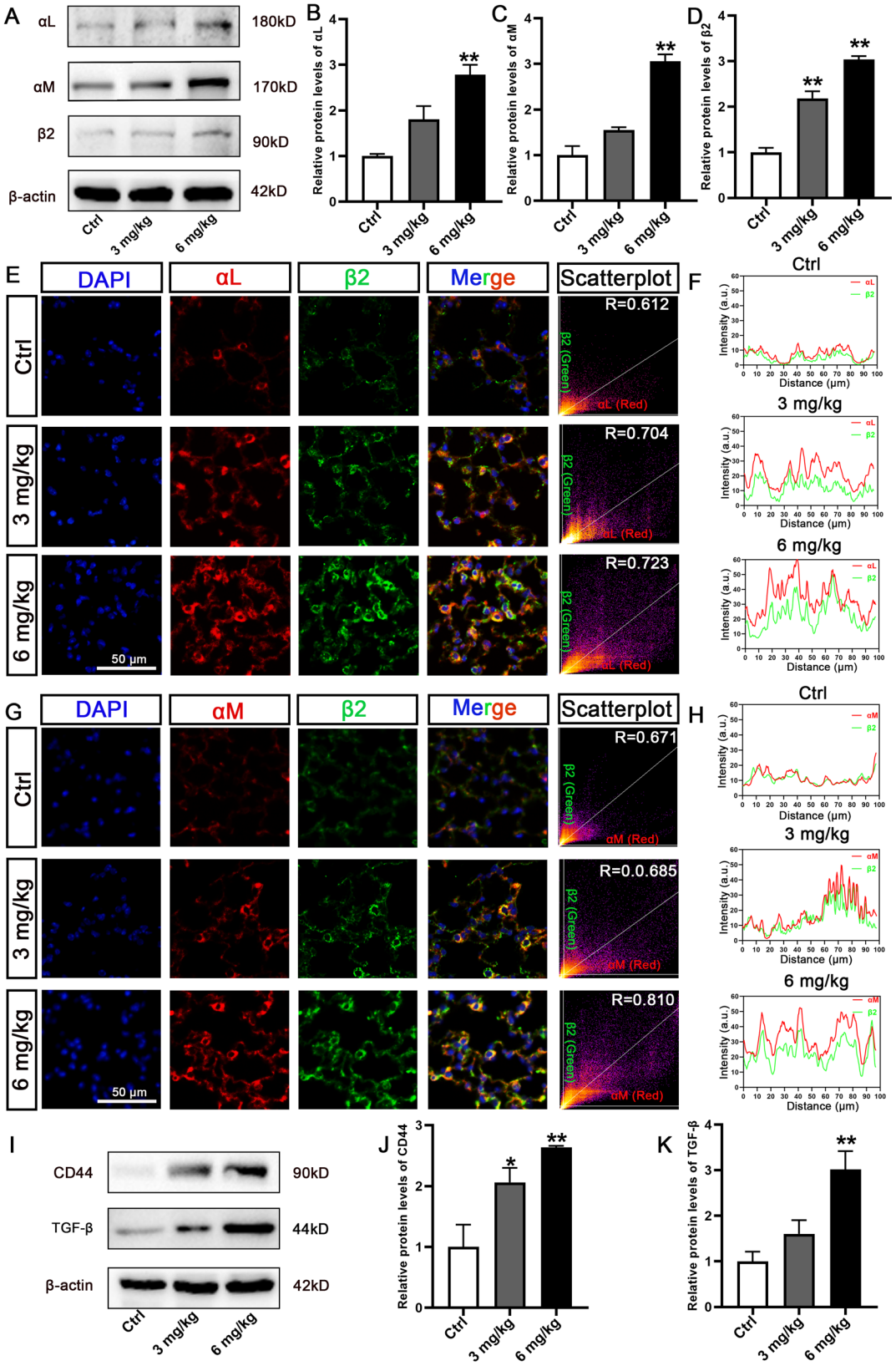

Fig. 6 Integrins, CD44 and TGF-β are involved in SiNPs-induced lung injury. (**A-D**) Western blotting analysis of integrin subunits αL, αM and β2 protein levels in lung tissues ($n = 3$). (**E-H**) Immunofluorescence of integrin subunits αL and β2, αM and β2 in lung tissues (scale bar = 50 μm). (**I-K**) Protein levels of CD44 and TGF-β in lung tissues ($n = 3$). Data are expressed as the mean ± *SD*. * $P < 0.05$, ** $P < 0.01$, vs. Ctrl group

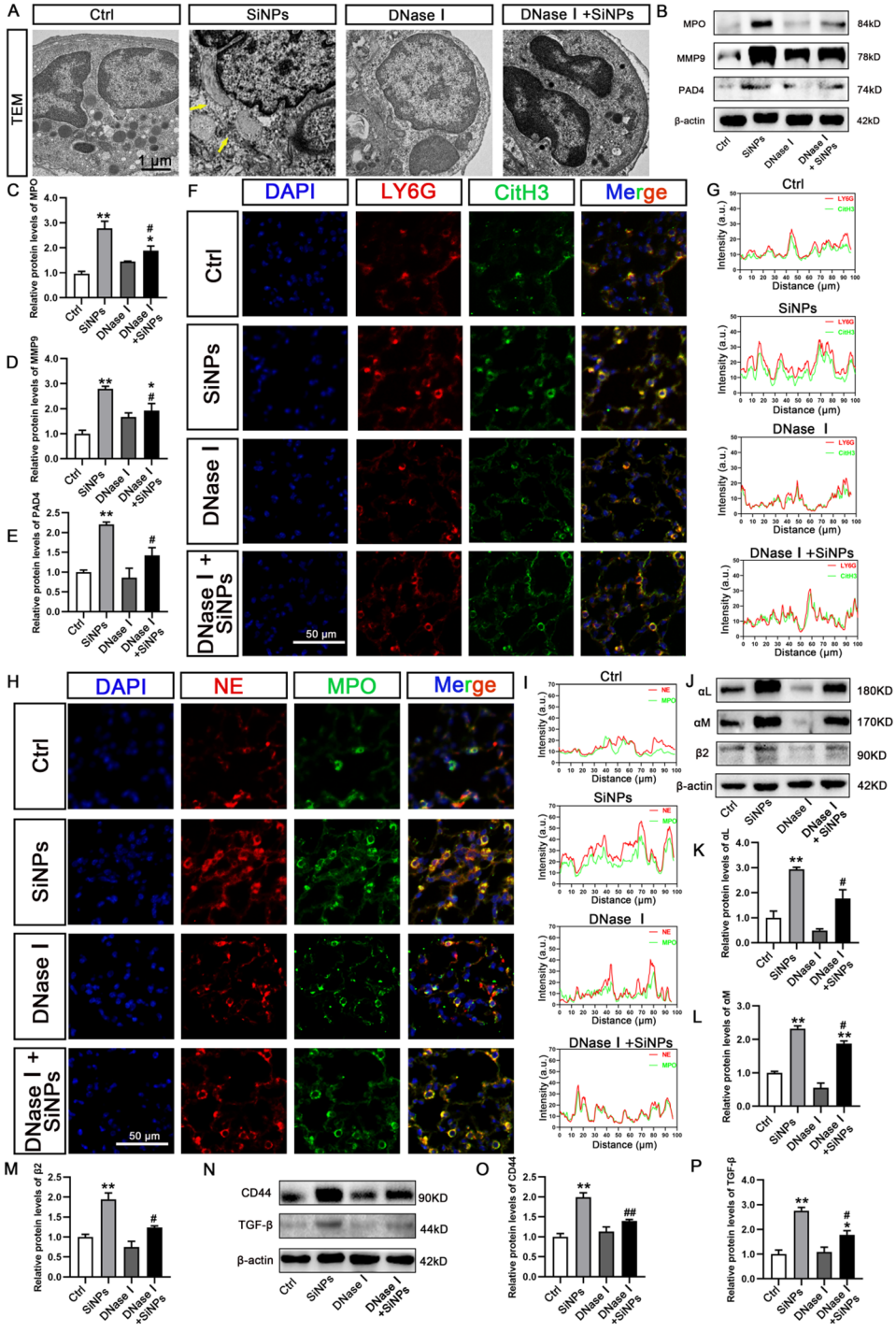

Fig. 7 Effect of NETs inhibitor DNase I on NETs, integrins, CD44 and TGF-β. (**A**) TEM of lung tissue. (yellow arrows: the disrupted cell membrane, scale bar = 1 μm). (**B-E**) Western blotting analysis of MPO, MMP9, and PAD4 protein levels in lung tissues ($n = 3$). (**F**) Immunofluorescence staining for CitH3 and LY6G in lung tissues (scale bar = 50 μm). (**G**) Immunofluorescence staining for MPO and NE in lung tissues (scale bar = 50 μm). (**H-I**) Analysis of the colocalization of red and green fluorescence. (**J-M**) Western blotting analysis of integrin subunits αL, αM and β2 protein levels in lung tissues ($n = 3$). (**N-P**) Western blotting analysis of CD44 and TGF-β protein levels in lung tissues ($n = 3$). Data are expressed as the mean ± *SD*. * $P < 0.05$, ** $P < 0.05$, vs. Ctrl group; # $P < 0.05$, ## $P < 0.01$, vs. SiNPs group

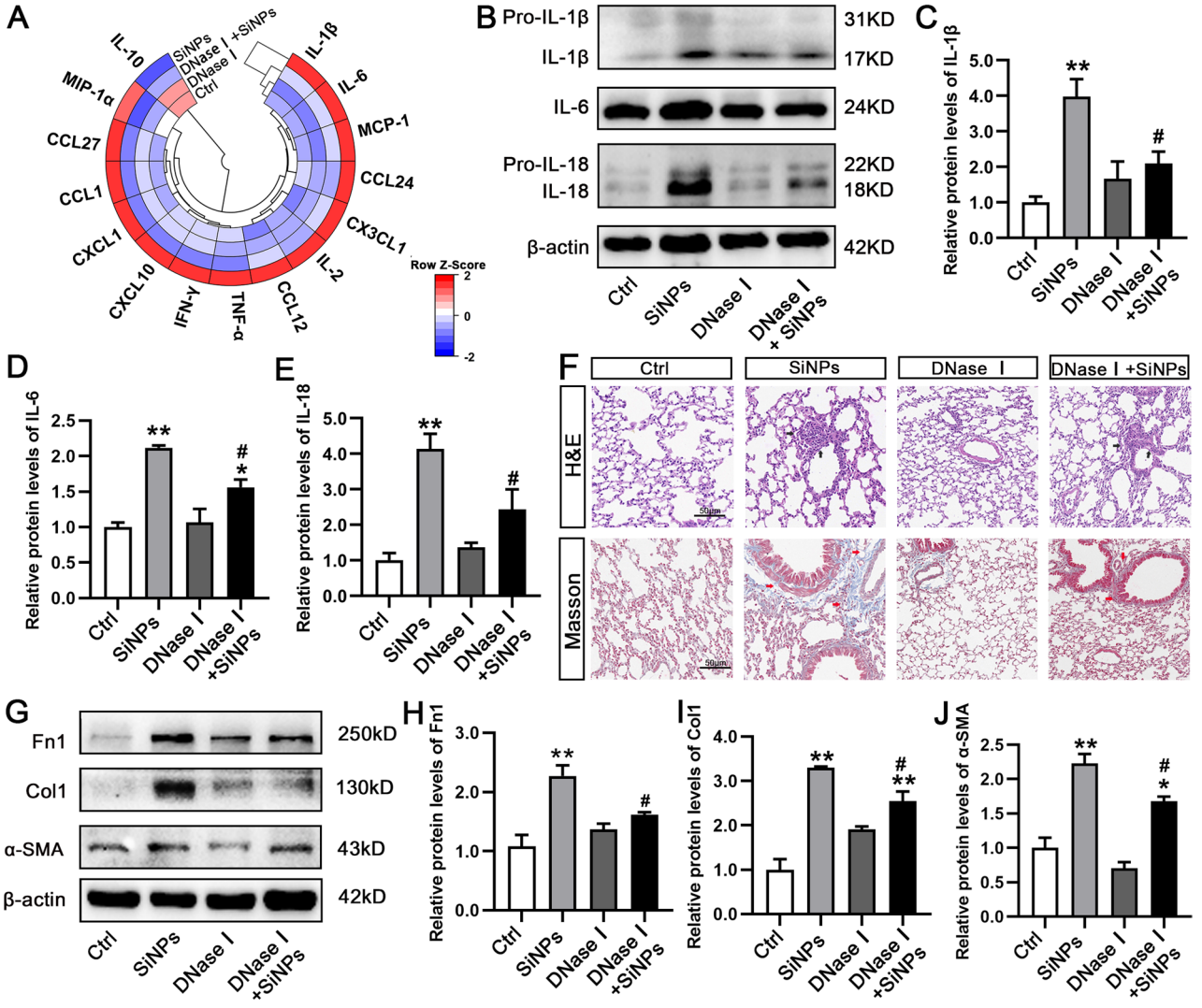

Fig. 8 The alleviation function of DNase I on SiNPs-induced lung injury. (**A**) Luminex multifactor detection of cytokines in BALF across all groups. The heatmap shows clustering based on average linkage performed by Origin's Polar Heatmapper Dendrogram plugin. The Z-Score indicates the deviation from the average level of the marker across groups, higher Z-scores are indicated in red and lower Z-scores in blue. 0 represents the cytokine's mean expression across groups, while + 2/−2 indicate one standard deviation above/below the mean, respectively. (**B-E**) Western blotting analysis of protein levels for IL-1β, IL-6 and IL-18 in lung tissues ($n = 3$). (**F**) H&E and Masson's trichrome staining of mice lungs (black arrows: inflammatory cell infiltration; red arrows: collagen deposition, scale bar = 50 μm). (**G-J**) Western blotting analysis of Fn1, Col1 and α-SMA in lung tissues ($n = 3$). Data are expressed as the mean ± *SD*. * $P < 0.05$, ** $P < 0.01$, vs. Ctrl group; # $P < 0.05$ vs. SiNPs group

demonstrated that DNase Ⅰ attenuated SiNPs-induced inflammatory cell infiltration and lung injury (Fig. 8F). Examination of lung tissue fibrosis also showed reduced expression of Fn1, Col1, and α-SMA, as well as decreased collagen deposition in the DNase Ⅰ + SiNPs group relative to the SiNPs group ($P < 0.05$, Fig. 8F-J). These results conclude that DNase I-meditated degradation of NETs could ameliorate SiNPs-induced lung injury.

Discussion

SiNPs are manufactured and utilized in substantial quantities, with inhalation through the respiratory tract representing the primary route of exposure to SiNPs in occupational settings. However, most current studies focus on assessing the safety and efficacy of oral and intravenous administration as a pharmaceutical vehicle. In contrast, the investigation of respiratory exposure toxicity in occupational settings represents a relatively underdeveloped area of research. In a study conducted by Fabio et al. at a site producing silica particles of 20, 50, and 100 nm in size, the exposure particle sizes were measured within a distance of 1.5 m adjacent to the work area (near field) and within a 0.3 m radius around the worker's nose and mouth (personal breathing zone). The findings revealed that workers were predominantly exposed to 80 nm silica particles during the production

process, which included synthesis in liquid, washing, and dryer opening [41]. The administered dose (3 mg/kg and 6 mg/kg) and frequency (once a week for 12 weeks) of SiNPs were based on inhalation studies in mice, in which the doses were evaluated in accordance with the actual occupational exposure scenarios [7, 31, 42]. Accordingly, the present study utilizes an animal model to simulate both the particle size and dose of occupational exposure, thereby providing evidence for the toxic mechanism of occupational lung injury induced by SiNPs.

Previous studies found that inhalation of SiNPs causes multisystem injury [32] and elicits a more severe inflammatory response than crystalline silica [43]. Neutrophils, the predominant innate immune cells, originate from the bone marrow and constitute 50–70% of circulating leukocytes in humans. They serve a multitude of specialized functions as effector of the innate immune response and as the primary defense mechanism against invading pathogens [44]. Under pathological conditions, prolonged infiltration of neutrophils can lead to chronic inflammation and tissue damage by interacting with and instructing other immune cells [45]. The recruitment of neutrophils in the airways and lungs is a major hallmark of many respiratory diseases [46, 47]. Workers exposed to SiNPs developed pulmonary inflammation and fibrosis, accompanied by an elevated neutrophil count [47, 48]. Meanwhile, in animal models in this study, lung injury was observed, and the number of neutrophils specifically labeled with LY6G immunofluorescence markers was significantly increased (Fig. 5F). These findings indicate that neutrophils may be a significant contributor to the development of lung injury induced by SiNPs. Complete neutrophil depletion or substantial reduction in neutrophil numbers leads to fatality or severe immunodeficiency in humans, making it unfeasible to treat for respiratory diseases clinically [49]. Therefore, it is crucial to investigate the mechanism by which neutrophils contribute to disease progression. NETs are web-like substances released by neutrophils. A substantial body of evidence suggests that the overproduction of NETs may exert direct cytotoxic effects on lung cells and accelerate the progression of both acute and chronic respiratory diseases [19, 46, 50, 51]. Several types of nanoparticles, including gold, silver, cationic lipids, polystyrene, nano-diamonds, and graphene oxide, have been shown to trigger the release of NETs, which play a critical role in innate immunity and inflammation [52]. Our study demonstrates the increased release of NETs in lung tissue following occupational exposure to SiNPs.

NETs likely exert distinct, exposure-dependent roles in acute and chronic respiratory injury [46]. Although a recent study implicated NETs in acute lung inflammatory injury induced by SiNPs exposure (40 μg/g bw) [23], the underlying regulatory mechanisms may differ substantially in this acute, high-dose exposure and in our occupational (subchronic, lower-dose) exposure model. In acute settings, rapid and transient NET release contributes to confine noxious stimuli. However, excessive or poorly resolved NETs disrupt the alveolar–capillary barrier, amplify epithelial and endothelial injury, and promote immunothrombosis, thereby aggravating gas-exchange failure [53–55]. Although Kusaka et al. showed that NADPH oxidase 2 (NOX2) inhibition suppresses NET formation and mitigates acute SiNPs-induced lung injury, NET-directed inhibit in acute disease warrants caution because NETs contribute to early antimicrobial defense; strategies should therefore modulate pathogenic NET activity without compromising host protection [23, 53, 56]. In chronic or subchronic contexts, persistent or recurrent NETs burden increases mucus viscoelasticity, sustains low-grade inflammation, and engages profibrotic pathways such as TGF-β activation, driving airway remodeling and fibrosis; interventions should prioritize enhancing NET clearance or neutralizing cytotoxic NET components to relieve obstruction and prevent ongoing inflammation and fibrosis [54, 57]. Differences in NETs responses between acute and chronic injury may reflect a shift in neutrophil activation phenotype. The latest study indicates that in the early phase of ALI, lung tissue exhibits and extensive neutrophil recruitment dominated by Siglec-F- cells. From 48 to 72 h the lung enters a reparative phase: total neutrophil numbers decline and a Siglec-F + neutrophil subset emerges, which secretes significantly lower levels of MPO, a NET-associated protein, and appears to contribute to the resolution of inflammatory injury [58]. In an idiopathic pulmonary fibrosis (IPF) model, Siglec-F+ neutrophils were increased and promoted NETs release, thereby contributing to the pathogenesis of pulmonary fibrosis [59]. The regulation of neutrophil phenotype and the role of NETs in acute versus chronic diseases merit further investigation. Although the upstream and downstream regulatory mechanisms of NETs in acute and chronic respiratory diseases remain incompletely understood, the foregoing studies collectively indicate that NETs constitute a promising therapeutic target to halt progressive inflammation and fibrosis.

NETs inhibitors can be classified into two principal categories: those that impede the formation of NETs and those that facilitate their degradation [60]. The efficacy of inhibiting NETs formation and promoting NETs degradation in respiratory diseases has been documented in the literature [61]. Emma et al. demonstrated that, in the complete absence of PAD4 (a major driver of NETs formation), while NET formation was inhibited, the severity of the pathogen load and inflammation in the lungs of mice was also increased [62]. In contrast, the degradation of NETs with DNase I was observed to reduce lung

injury and improve survival without interfering with the original physiological function of neutrophils or increasing the pathogen load in the lungs and bloodstream [62, 63]. Furthermore, the U.S. Food and Drug Administration (FDA) approved DNase I for cystic fibrosis patients decades ago, establishing its safety as a pharmaceutical agent [64]. In light of the aforementioned evidence, the present study employed DNase I as an intervention for NETs. These results indicate that DNase I effectively degrades NETs in the lungs of mice exposed to SiNPs and attenuates pulmonary inflammation and fibrotic injury.

Integrins are key transmembrane receptors that fulfill multiple functions in biochemical and mechanical signaling between cells and their extracellular environment and have been implicated in both health and disease states [65]. Especially, the β2 family are specifically expressed on leukocytes. Among the four integrin β2 families expressed on neutrophils, αLβ2 and αMβ2 are the two predominantly expressed types [24, 26]. Bioinformatics intersecting lung-injury and NETs gene sets highlighted integrins, and we observed increased expression and co-localization of the αLβ2 and αMβ2 (Figs. 3 and 6). Degrading NETs with DNase I reduced pulmonary NET burden and markedly suppressed αLβ2 and αMβ2 expression (Fig. 7). These findings imply that NETs may contribute to SiNPs-induced lung injury by modulating integrin expression under the specific conditions examined in this study. TGF-β is a pivotal activator of fibrotic responses. Cell biology studies, animal model experiments, and clinical evidences collectively support the essential role of TGF-β is in mediating tissue fibrosis [66, 67]. Integrins are well-established activators of latent TGF-β, this function is classically attributed to αV-containing integrins expressed on epithelial cells and fibroblasts [67–69]. Interventions targeting integrin-dependent TGF-β activation may offer an effective approach to prevent and treat fibrosis-related diseases [70–72]. DNase I exhibited a protective effect against fibrotic lung injury, and concurrently inhibited the SiNPs-induced upregulation of integrin αLβ2 and αMβ2 as well as TGF-β in this study. These results lead to the hypothesis that NETs may contribute to SiNPs-induced lung injury through the NETs/integrins/TGF-β signaling pathway.

NET components such as NE, MPO, and MMP9 can amplify cytokine production and recruit additional neutrophils, intensifying the inflammatory cycle [46, 54]. Our analyses indicate that in addition to the integrins family, inflammatory responses, chemokine activity, the TNF-α pathway and cellular responses to interleukins may also be associated with NETs in lung injury. Persistent inflammation is essential for the progression of pulmonary fibrosis. SiNPs could precipitate an elevation in inflammatory cytokines within BALF and lung tissue. CD44 - a widely expressed transmembrane receptor regulated by inflammatory mediators including MMP9, IL-1β, IFN-γ, TNF-α, and CXCL10 - has recognized roles in tissue injury and fibrogenesis [73–77]. CD44 blockade attenuates experimental liver and lung fibrosis [77–81]. We observed CD44 upregulation following SiNPs exposure, which was suppressed by DNase I together with reductions in the aforementioned inflammatory mediators. Based on these evidences, it seems reasonable to hypothesize that SiNPs may enhance cytokine secretion in lung tissue by facilitating the formation and release of NETs, which activate CD44, ultimately leading to the development of lung injury.

This study demonstrates that exposure to SiNPs at occupational doses leads to inflammatory and fibrotic lung damage in mice. NETs may be involved in SiNPs -induced lung injury via the NETs/integrins/TGF-β and NETs/cytokines/CD44 pathways. These findings underscore the significant role of NETs in lung injury induced by occupational exposure to SiNPs and highlight the potential value of inhibiting this process through therapeutic interventions. Notably, although DNase I has been used to modulate NETs in many disease models [82–86], including in this study, it is not NET-specific; it degrades extracellular DNA regardless of cellular origin. Therefore, our results provide only preliminary evidence regarding NET-related functions and mechanisms. Targeted experiments, such as cell-type-specific conditional knockout mice, NET-specific interventions, or nanomaterial-based, NET-targeted delivery systems [87], will be required to quantify the relative contributions of extracellular DNA derived from non-neutrophil cells versus NET clearance.

5. Conclusion

In summary, our findings suggest that NETs may play a role in SiNPs -induced inflammatory and fibrotic lung injuries via the NETs/integrins/TGF-β and NETs/cytokines/CD44 signaling pathways. Furthermore, we demonstrated a potential therapeutic strategy using DNase I, a NETs inhibitor, which could alleviate inflammatory responses and fibrogenesis by promoting NETs degradation (Fig. 9). Targeting NETs degradation may offer a novel therapeutic strategy for occupational SiNPs exposure -induced lung injury and could provide a potential therapeutic approach for inflammatory and fibrotic diseases. However, specific regulatory mechanisms and the clinical translation of targeted interventions for NETs remain to be further explored in vitro and in vivo studies, and in patients with SiNPs-induced lung injury.

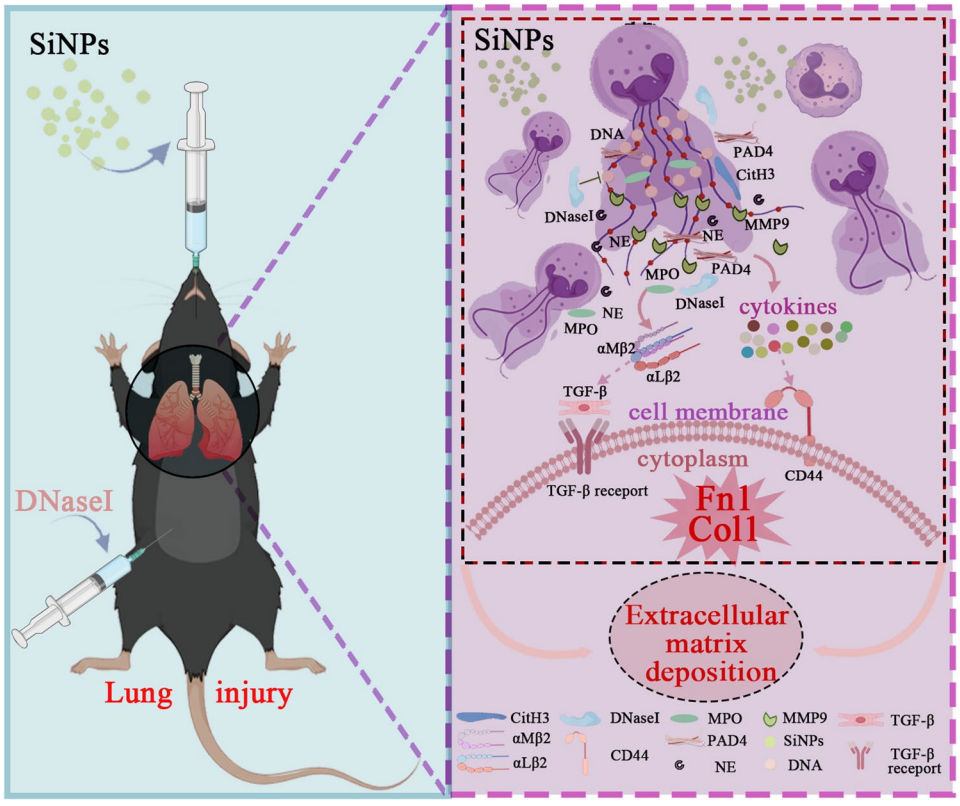

Fig. 9 Schematic of the mechanisms involved in NETs for silica nanoparticle-induced lung injury. SiNPs stimulate the formation and release of NETs components, which subsequently activate integrins/TGF-β, and cytokines/CD44, resulting in inflammatory and fibrotic injury to lung tissue. DNase I facilitates the degradation of NETs, thereby mitigating SiNPs-induced lung injury

Abbreviations

α-SMA	α-smooth muscle actin
BALF	Bronchoalveolar Lavage Fluid
BC	Betweenness Centrality
BCA	Bicinchoninic acid
BP	Biological processes
BSA	Bovine serum albumin
CAGR	Compound Average Growth Rate
CC	Cellular components
CCL12	Chemokine (C-C motif) ligand 12
CD18	Integrin subunit beta 2
CD44	Cluster of differentiation 44
CG	Cathepsin G
CitH3	Citrullination of histone H3
Col1	Type Ⅰ collagen
CTD	Comparative Toxicogenomics Database
CX3CL1	C-X3-Chemokine Ligand 1
CXCL1	C-X-C motif chemokine Ligand 1
CXCL10	C-X-C Motif Chemokine Ligand 10
DAPI	4′,6-diamidino-2-phenylindole
DC	Degree Centrality
DEGs	Differentially expressed genes
DNase I	Deoxyribonuclease I
ECM	Extracellular matrix
EMT	Epithelial-mesenchymal transition
FITC	Fluorescein isothiocyanate
FDA	Food and Drug Administration
Fn1	Fibronectin, GO: Gene Ontology
H&E	Hematoxylin and eosin
ILD	Interstitial Lung Disease
KEGG	Kyoto Encyclopedia of Genes and Genomes
LFA-1	Leukocyte Function-associated Antigen-1
MF	Molecular functions
MMP9	Matrix metalloproteinases 9
MPO	Myeloperoxidase
NE	Neutrophil elastase
NETs	Neutrophil extracellular traps
NRGs	Neutrophil extracellular trap-related genes
OMIM	Online Mendelian Inheritance in Man
PAD4	Protein-arginine deiminase type 4
PMSF	Phenylmethanesulfonyl fluoride
PPI	Protein-Protein Interaction Networks
PVDF	Polyvinylidene Fluoride
RIPA	Radio Immuno Precipitation Assay
SiNPs	Silica nanoparticles
TBST	Tris-Buffered Saline with Tween 20
TEM	Transmission Electron Microscope
TTD	Therapeutic Target Database

Supplementary Information

The online version contains supplementary material available at https://doi.org/10.1186/s12951-026-04415-0.

Supplementary Material 1.

Acknowledgements
Not applicable.

Author contributions
Xiu He: Conceptualization, Methodology, Investigation, Visualization, Writing – original draft, Funding acquisition. Xiaoli Yuan: Methodology, Visualization, Writing – original draft, Writing—review and editing. Xuedong Sa: Visualization, Writing – original draft, Writing—review and editing,

Investigation. Jiaqi Ban: Writing—review and editing, Supervision. Shuai Fu: Supervision, Investigation. Mingdan You : Funding acquisition. Jun Li: Conceptualization, Writing—review and editing, Supervision. All authors read and approved the final manuscript.

Funding
This study was supported by the National Natural Science Foundation of China (grant no. 82260635), the Excellent Young Talents Plan of Guizhou Medical University (grant no. 2023/108).

Data availability
The datasets generated and/or analysed during the current study are not publicly available due [REASON WHY DATA ARE NOT PUBLIC] but are available from the corresponding author on reasonable request.

Declarations

Ethics approval and consent to participate
All experiments were conducted in accordance with the guidelines of Guizhou Medical University for the care and use of laboratory animals and were approved by the Animal Ethical Committee of Guizhou Medical University [Number 2100247].

Consent for publication
Not applicable.

Competing interests
The authors declare no competing interests.

Author details
[1]School of Public Health, the Key Laboratory of Environmental Pollution Monitoring and Disease Control, Ministry of Education, Guizhou Medical University, Guiyang 561113, China

Received: 14 November 2025 / Accepted: 1 April 2026
Published online: 14 April 2026

References

1. Newswire P. Nanotechnology Products Market size is set to grow by USD 161.3 billion from 2024–2028, Increasing adoption of novel nanotechnology tools to boost agricultural productivity boost the market, Technavio 2024 [cited 2024 Oct 29]. Available from: https://www.prnewswire.com/news-releases/nanotechnology-products-market-size-is-set-to-grow-by-usd-161-3-billion-from-2024-2028--increasing-adoption-of-novel-nanotechnology-tools-to-boost-agricultural-productivity-boost-the-market-technavio-302197051.html
2. Najahi-Missaoui W, Arnold RD, Cummings BS. Safe Nanoparticles: Are We There Yet?. Int J Mol Sci. 2020;22(1):385.
3. Ali M. What function of nanoparticles is the primary factor for their hypertoxicity? Adv Colloid Interface Sci. 2023;314:102881.
4. Guo C, Liu Y, Li Y. Adverse effects of amorphous silica nanoparticles: Focus on human cardiovascular health. J Hazard Mater. 2021;406:124626.
5. Guo C, Zhao X, Ma R, Zhu L, Chen Y, Yang Z, et al. Silica nanoparticles promoted pro-inflammatory macrophage and foam cell transformation via ROS/PPARγ/NF-κB signaling. Sci Total Environ. 2023;881:163430.
6. Wei W, Yan Z, Liu X, Qin Z, Tao X, Zhu X, et al. Brain Accumulation and Toxicity Profiles of Silica Nanoparticles: The Influence of Size and Exposure Route. Environ Sci Technol. 2022;56(12):8319–25.
7. Abulikemu A, Zhao X, Xu H, Li Y, Ma R, Yao Q, et al. Silica nanoparticles aggravated the metabolic associated fatty liver disease through disturbed amino acid and lipid metabolisms-mediated oxidative stress. Redox Biol. 2023;59:102569.
8. Liu N, Li M, Pang H, Tiantian T, Li X, Su Y, et al. Bioinformatics-driven discovery of silica nanoparticles induces apoptosis and renal damage via the unfolded protein response in NRK-52E cells and rat kidney. Comput Biol Med. 2024;168:107816.
9. Wang M, Li J, Dong S, Cai X, Simaiti A, Yang X, et al. Silica nanoparticles induce lung inflammation in mice via ROS/PARP/TRPM2 signaling-mediated lysosome impairment and autophagy dysfunction. Part Fibre Toxicol. 2020;17(1):23.
10. Ao LH, Wei YG, Tian HR, Zhao H, Li J, Ban JQ. Advances in the study of silica nanoparticles in lung diseases. Sci Total Environ. 2024;912:169352.
11. Zhao X, Wei S, Li Z, Lin C, Zhu Z, Sun D, et al. Autophagic flux blockage in alveolar epithelial cells is essential in silica nanoparticle-induced pulmonary fibrosis. Cell Death Dis. 2019;10(2):127.
12. Li DD, Zheng CQ, Zhang F, Shi JS. Potential neuroprotection by Dendrobium nobile Lindl alkaloid in Alzheimer's disease models. Neural regeneration Res. 2022;17(5):972–7.
13. Kanashiro A, Hiroki CH, da Fonseca DM, Birbrair A, Ferreira RG, Bassi GS, et al. The role of neutrophils in neuro-immune modulation. Pharmacol Res. 2020;151:104580.
14. Suzuki M, Ikari J, Anazawa R, Tanaka N, Katsumata Y, Shimada A, et al. PAD4 Deficiency Improves Bleomycin-induced Neutrophil Extracellular Traps and Fibrosis in Mouse Lung. Am J Respir Cell Mol Biol. 2020;63(6):806–18.
15. Adrover JM, McDowell SAC, He XY, Quail DF, Egeblad M. NETworking with cancer: The bidirectional interplay between cancer and neutrophil extracellular traps. Cancer Cell. 2023;41(3):505–26.
16. Zhao J, Zhen N, Zhou Q, Lou J, Cui W, Zhang G et al. NETs Promote Inflammatory Injury by Activating cGAS-STING Pathway in Acute Lung Injury. Int J Mol Sci. 2023;24(6):5125.
17. Scozzi D, Liao F, Krupnick AS, Kreisel D, Gelman AE. The role of neutrophil extracellular traps in acute lung injury. Front Immunol. 2022;13:953195.
18. Burkard P, Schonhart C, Vögtle T, Köhler D, Tang L, Johnson D, et al. A key role for platelet GPVI in neutrophil recruitment, migration, and NETosis in the early stages of acute lung injury. Blood. 2023;142(17):1463–77.
19. Lachowicz-Scroggins ME, Dunican EM, Charbit AR, Raymond W, Looney MR, Peters MC, et al. Extracellular DNA, Neutrophil Extracellular Traps, and Inflammasome Activation in Severe Asthma. Am J Respir Crit Care Med. 2019;199(9):1076–85.
20. Chen J, Wang T, Li X, Gao L, Wang K, Cheng M, et al. DNA of neutrophil extracellular traps promote NF-κB-dependent autoimmunity via cGAS/TLR9 in chronic obstructive pulmonary disease. Signal Transduct Target therapy. 2024;9(1):163.
21. Katsoulis O, Toussaint M, Jackson MM, Mallia P, Footitt J, Mincham KT, et al. Neutrophil extracellular traps promote immunopathogenesis of virus-induced COPD exacerbations. Nat Commun. 2024;15(1):5766.
22. Ma Q, Steiger S. Neutrophils and extracellular traps in crystal-associated diseases. Trends Mol Med. 2024;30(9):809–23.
23. Kusaka M, Sakamoto K, Ikeyama Y, Kondo Y, Hayashi T, Ando A, et al. NOX2-Dependent Phagocyte Signaling Mediates Silica-Induced Murine Lung Injury via Macrophage-Neutrophil Interactions. Inflammation. 2025;49(1):3.
24. Pulikkot S, Hu L, Chen Y, Sun H, Fan Z. Integrin Regulators in Neutrophils. Cells. 2022;11(13):2025.
25. O'Brien XM, Reichner JS. Neutrophil Integrins and Matrix Ligands and NET Release. Front Immunol. 2016;7:363.
26. Torres-Gomez A, Cabañas C, Lafuente EM. Phagocytic Integrins: Activation and Signaling. Front Immunol. 2020;11:738.
27. Raftery MJ, Lalwani P, Krautkrämer E, Peters T, Scharffetter-Kochanek K, Krüger R, et al. β2 integrin mediates hantavirus-induced release of neutrophil extracellular traps. J Exp Med. 2014;211(7):1485–97.
28. Khawaja AA, Chong DLW, Sahota J, Mikolasch TA, Pericleous C, Ripoll VM, et al. Identification of a Novel HIF-1α-α(M)β(2) Integrin-NET Axis in Fibrotic Interstitial Lung Disease. Front Immunol. 2020;11:2190.
29. Mousset A, Lecorgne E, Bourget I, Lopez P, Jenovai K, Cherfils-Vicini J, et al. Neutrophil extracellular traps formed during chemotherapy confer treatment resistance via TGF-β activation. Cancer Cell. 2023;41(4):757–e7510.
30. Albrengues J, Shields MA, Ng D, Park CG, Ambrico A, Poindexter ME, et al. Neutrophil extracellular traps produced during inflammation awaken dormant cancer cells in mice. Volume 361. New York, NY: Science; 2018. 6409.
31. Ma R, Qi Y, Zhao X, Li X, Sun X, Niu P, et al. Amorphous silica nanoparticles accelerated atherosclerotic lesion progression in ApoE(-/-) mice through endoplasmic reticulum stress-mediated CD36 up-regulation in macrophage. Part Fibre Toxicol. 2020;17(1):50.
32. Ban JQ, Ao LH, Gu HQ, Wei YG, Tian Q, He X, et al. From inhalation to systemic damage: Decoding the mechanistic cascade of silica nanoparticle-induced multi-organ toxicity. Toxicology. 2026;519:154310.
33. He X, Chen S, Li C, Ban J, Wei Y, He Y, et al. Trehalose Alleviates Crystalline Silica-Induced Pulmonary Fibrosis via Activation of the TFEB-Mediated Autophagy-Lysosomal System in Alveolar Macrophages. Cells. 2020;9(1):122.
34. Li S, Li C, Zhang Y, He X, Chen X, Zeng X, et al. Targeting Mechanics-Induced Fibroblast Activation through CD44-RhoA-YAP Pathway Ameliorates Crystalline Silica-Induced Silicosis. Theranostics. 2019;9(17):4993–5008.

35. He X, Chen S, Li C, Ban J, Wei Y, He Y et al. Trehalose Alleviates Crystalline Silica-Induced Pulmonary Fibrosis via Activation of the TFEB-Mediated Autophagy-Lysosomal System in Alveolar Macrophages. Cells. 2020;9(1):122.
36. Mikawa K, Nishina K, Takao Y, Obara H. ONO-1714, a nitric oxide synthase inhibitor, attenuates endotoxin-induced acute lung injury in rabbits. Anesth Analg. 2003;97(6):1751–5.
37. Hübner RH, Gitter W, El Mokhtari NE, Mathiak M, Both M, Bolte H, et al. Standardized quantification of pulmonary fibrosis in histological samples. Biotechniques. 2008;44(4):507–11. 14 – 7.
38. Jiang T, Wang Y, Chen X, Xia W, Xue S, Gu L, et al. Neutrophil extracellular traps (NETs)-related lncRNAs signature for predicting prognosis and the immune microenvironment in breast cancer. Front cell Dev biology. 2023;11:1117637.
39. Zhang Y, Guo L, Dai Q, Shang B, Xiao T, Di X et al. A signature for pan-cancer prognosis based on neutrophil extracellular traps. J Immunother Cancer. 2022;10(6):e004210.
40. van Hooij A, van Meijgaarden KE, Khatun M, Soren S, Walburg K, Alam K, et al. Integrative immune analysis in patients with leprosy reveals host factors associated with mycobacterial control. EBioMedicine. 2025;118:105855.
41. Boccuni F, Ferrante R, Tombolini F, Natale C, Gordiani A, Sabella S, et al. Occupational exposure to graphene and silica nanoparticles. Part I: workplace measurements and samplings. Nanotoxicology. 2020;14(9):1280–300.
42. You R, Ho YS, Hung CH, Liu Y, Huang CX, Chan HN, et al. Silica nanoparticles induce neurodegeneration-like changes in behavior, neuropathology, and affect synapse through MAPK activation. Part Fibre Toxicol. 2018;15(1):28.
43. Chen L, Liu J, Zhang Y, Zhang G, Kang Y, Chen A, et al. The toxicity of silica nanoparticles to the immune system. Nanomed (London England). 2018;13(15):1939–62.
44. Pérez-Figueroa E, Álvarez-Carrasco P, Ortega E, Maldonado-Bernal C. Neutrophils: Many Ways to Die. Front Immunol. 2021;12:631821.
45. Carnevale S, Di Ceglie I, Grieco G, Rigatelli A, Bonavita E, Jaillon S. Neutrophil diversity in inflammation and cancer. Front Immunol. 2023;14:1180810.
46. Keir HR, Chalmers JD. Neutrophil extracellular traps in chronic lung disease: implications for pathogenesis and therapy. Eur respiratory review: official J Eur Respiratory Soc. 2022;31(163):210241.
47. Cortjens B, van Woensel JB, Bem RA. Neutrophil Extracellular Traps in Respiratory Disease: guided anti-microbial traps or toxic webs? Paediatr Respir Rev. 2017;21:54–61.
48. Liao HY, Chung YT, Lai CH, Wang SL, Chiang HC, Li LA, et al. Six-month follow-up study of health markers of nanomaterials among workers handling engineered nanomaterials. Nanotoxicology. 2014;8(Suppl 1):100–10.
49. Liew PX, Kubes P. The Neutrophil's Role During Health and Disease. Physiol Rev. 2019;99(2):1223–48.
50. Liu X, Li T, Chen H, Yuan L, Ao H. Role and intervention of PAD4 in NETs in acute respiratory distress syndrome. Respir Res. 2024;25(1):63.
51. Ackermann M, Anders HJ, Bilyy R, Bowlin GL, Daniel C, De Lorenzo R, et al. Patients with COVID-19: in the dark-NETs of neutrophils. Cell Death Differ. 2021;28(11):3125–39.
52. Yang H, Marion TN, Liu Y, Zhang L, Cao X, Hu H, et al. Nanomaterial Exposure Induced Neutrophil Extracellular Traps: A New Target in Inflammation and Innate Immunity. J Immunol Res. 2019;2019:3560180.
53. Kenny EF, Herzig A, Krüger R, Muth A, Mondal S, Thompson PR et al. Diverse stimuli engage different neutrophil extracellular trap pathways. eLife. 2017;6:e24437.
54. Papayannopoulos V. Neutrophil extracellular traps in immunity and disease. Nat Rev Immunol. 2018;18(2):134–47.
55. Middleton EA, He XY, Denorme F, Campbell RA, Ng D, Salvatore SP, et al. Neutrophil extracellular traps contribute to immunothrombosis in COVID-19 acute respiratory distress syndrome. Blood. 2020;136(10):1169–79.
56. Jorch SK, Kubes P. An emerging role for neutrophil extracellular traps in noninfectious disease. Nat Med. 2017;23(3):279–87.
57. Murugadoss S, Lison D, Godderis L, Van Den Brule S, Mast J, Brassinne F, et al. Toxicology of silica nanoparticles: an update. Arch Toxicol. 2017;91(9):2967–3010.
58. Tavares LP, Brüggemann TR, Cagnina RE, Nshimiyimana R, Villaseñor-Altamirano AB, Rezende RM, et al. Siglec-F(+) neutrophils promote the resolution of acute lung injury through ALOX15 induction. Sci Immunol. 2025;10(114):eaeb2657.
59. Hiroki CH, Hassanabad MF, Defaye M, Sarden N, Bartlett A, Farias R et al. Nociceptor neurons suppress alveolar macrophage-induced Siglec-F(+) neutrophil-mediated inflammation to protect against pulmonary fibrosis. Immunity. 2025;58(8):2054-68.e6.
60. Jo A, Kim DW. Neutrophil Extracellular Traps in Airway Diseases: Pathological Roles and Therapeutic Implications. Int J Mol Sci. 2023;24(5).
61. Xia M, Xu F, Ni H, Wang Q, Zhang R, Lou Y, et al. Neutrophil activation and NETosis are the predominant drivers of airway inflammation in an OVA/CFA/LPS induced murine model. Respir Res. 2022;23(1):289.
62. Lefrançais E, Mallavia B, Zhuo H, Calfee CS, Looney MR. Maladaptive role of neutrophil extracellular traps in pathogen-induced lung injury. JCI insight. 2018;3(3):e98178.
63. Chamardani TM, Amiritavassoli S. Inhibition of NETosis for treatment purposes: friend or foe?. Molecular Cellular Biochem. 2022;477(3):673–88.
64. Gray RD, McCullagh BN, McCray PB. NETs and CF Lung Disease: Current Status and Future Prospects. Antibiot (Basel Switzerland). 2015;4(1):62–75.
65. Pang X, He X, Qiu Z, Zhang H, Xie R, Liu Z, et al. Targeting integrin pathways: mechanisms and advances in therapy. Signal Transduct Target therapy. 2023;8(1):1.
66. Lafyatis R. Transforming growth factor β--at the centre of systemic sclerosis. Nat Rev Rheumatol. 2014;10(12):706–19.
67. Frangogiannis N. Transforming growth factor-β in tissue fibrosis. J Exp Med. 2020;217(3):e20190103.
68. Cao Y, Su H, Zeng J, Xie Y, Liu Z, Liu F, et al. Integrin β8 prevents pericyte-myofibroblast transition and renal fibrosis through inhibiting the TGF-β1/TGFBR1/Smad3 pathway in diabetic kidney disease. Translational research: J Lab Clin Med. 2024;265:36–50.
69. Chen X, Li X, Wu X, Ding Y, Li Y, Zhou G, et al. Integrin beta-like 1 mediates fibroblast-cardiomyocyte crosstalk to promote cardiac fibrosis and hypertrophy. Cardiovascular Res. 2023;119(10):1928–41.
70. Leask A, Fadl A, Naik A. A modest proposal: targeting αv integrin-mediated activation of latent TGFbeta as a novel therapeutic approach to treat scleroderma fibrosis. Expert Opin Investig Drugs. 2024;33(3):279–85.
71. Sime P, Jenkins G. Goldilocks and the Three Trials: Clinical Trials Targeting the α(v)β(6) Integrin in Idiopathic Pulmonary Fibrosis. Am J Respir Crit Care Med. 2022;206(9):1062–3.
72. Huang Y, Zhao H, Zhang Y, Tang Y, Shi X, Jiang S, et al. Enhancement of Zyxin Promotes Skin Fibrosis by Regulating FAK/PI3K/AKT and TGF-β Signaling Pathways via Integrins. Int J Biol Sci. 2023;19(8):2394–408.
73. Lin KC, Wu CC, Mokgautsi N, Lawal B, Wu CZ, Wu AT, et al. In silico repurposing of midostaurin as a therapeutic candidate for head and neck cancer via targeting SPARC/MMP9/CD44 Cancer-Associated Fibroblasts (CAFs) oncogenic signature. Am J cancer Res. 2023;13(3):1004–25.
74. Veschi V, Turdo A, Modica C, Verona F, Di Franco S, Gaggianesi M, et al. Recapitulating thyroid cancer histotypes through engineering embryonic stem cells. Nat Commun. 2023;14(1):1351.
75. Leir SH, Holgate ST, Lackie PM. Inflammatory cytokines can enhance CD44-mediated airway epithelial cell adhesion independently of CD44 expression. Am J Physiol Lung Cell Mol Physiol. 2003;285(6):L1305–11.
76. Han J, Lee C, Jeong H, Jeon S, Lee M, Lee H, et al. Tumor necrosis factor-inducible gene 6 protein and its derived peptide ameliorate liver fibrosis by repressing CD44 activation in mice with alcohol-related liver disease. J Biomed Sci. 2024;31(1):54.
77. Cheng D, Lian W, Wang T, Xi S, Jia X, Li Z, et al. The interplay of Cxcl10(+)/Mmp14(+) monocytes and Ccl3(+) neutrophils proactively mediates silica-induced pulmonary fibrosis. J Hazard Mater. 2024;467:133713.
78. Li Y, Jiang D, Liang J, Meltzer EB, Gray A, Miura R, et al. Severe lung fibrosis requires an invasive fibroblast phenotype regulated by hyaluronan and CD44. J Exp Med. 2011;208(7):1459–71.
79. Chi JY, Hsiao YW, Liang HY, Huang TH, Chen FW, Chen CY et al. Blockade of the pentraxin 3/CD44 interaction attenuates lung injury-induced fibrosis.Clin Transl Med. 2022;12(11):e1099.
80. Gong L, Zhou H, Zhang S, Wang C, Fu K, Ma C, et al. CD44-Targeting Drug Delivery System of Exosomes Loading Forsythiaside A Combats Liver Fibrosis via Regulating NLRP3-Mediated Pyroptosis. Adv Healthc Mater. 2023;12(11):e2202228.
81. Li Y, Zhang T, Zhang J, Liu Q, Jia Q, Chen W, et al. Dually fibronectin/CD44-mediated nanoparticles targeted disrupt the Golgi apparatus and inhibit the hedgehog signaling in activated hepatic stellate cells to alleviate liver fibrosis. Biomaterials. 2023;301:122232.
82. He XY, Gao Y, Ng D, Michalopoulou E, George S, Adrover JM, et al. Chronic stress increases metastasis via neutrophil-mediated changes to the microenvironment. Cancer Cell. 2024;42(3):474–e8612.
83. Xia Y, Wang Y, Xiong Q, He J, Wang H, Islam M, et al. Neutrophil extracellular traps promote MASH fibrosis by metabolic reprogramming of HSC. Hepatology (Baltimore MD). 2025;81(3):947–61.

84. Wang R, Zhu Y, Liu Z, Chang L, Bai X, Kang L, et al. Neutrophil extracellular traps promote tPA-induced brain hemorrhage via cGAS in mice with stroke. Blood. 2021;138(1):91–103.
85. Tsai CH, Lai AC, Lin YC, Chi PY, Chen YC, Yang YH, et al. Neutrophil extracellular trap production and CCL4L2 expression influence corticosteroid response in asthma. Sci Transl Med. 2023;15(699):eadf3843.
86. Wei X, Zou S, Xie Z, Wang Z, Huang N, Cen Z, et al. EDIL3 deficiency ameliorates adverse cardiac remodelling by neutrophil extracellular traps (NET)-mediated macrophage polarization. Cardiovascular Res. 2022;118(9):2179–95.
87. Lee HJ, Lee NK, Kim J, Kim J, Seo D, Shin HE, et al. Sequential nanoparticle therapy targeting neutrophil hyperactivation to prevent neutrophil-induced pulmonary fibrosis. J Nanobiotechnol. 2025;23(1):381.

Publisher's note